Magnetic Resonance Imaging 63 (2019) 85–92

Contents lists available at ScienceDirect

Magnetic Resonance Imaging

journal homepage: www.elsevier.com/locate/mri

Original contribution

A new technique for motion encoding gradient-less MR elastography of the psoas major muscle: A gradient-echo type multi-echo sequence

Tomokazu Numano[a,b,*], Tetsushi Habe[a], Daiki Ito[a,b,c], Takaaki Onishi[a], Koichi Takamoto[d], Kazuyuki Mizuhara[e], Hisao Nishijo[d], Keisuke Igarashi[a], Takamichi Ueki[a]

[a] Department of Radiological Science, Graduate School of Human Health Science, Tokyo Metropolitan University, Japan
[b] Human Technology Research Institute, National Institute of Advanced Industrial Science and Technology (AIST), Japan
[c] Office of Radiation Technology, Keio University Hospital, Japan
[d] System Emotional Science, Graduate School of Medicine and Pharmaceutical Sciences, University of Toyama, Japan
[e] Department of Mechanical Engineering, Tokyo Denki University, Japan

ARTICLE INFO

Keywords:
MR elastography
Psoas major muscle
Motion encoding gradient
Multi-echo sequence
Wave propagation
Muscle fibers

ABSTRACT

The present study aimed to develop vibration techniques for magnetic resonance (MR) elastography (MRE) of the psoas major muscle (PM). Seven healthy volunteers were included. MRE was performed with motion-encoding gradient (MEG)-less multi-echo MRE sequence, which allows clinicians to perform MRE using conventional MR imaging. In order to transmit mechanical vibration of the pneumatic type to the PM, a long narrow vibration pad was designed using a 3D printer, and the optimum vibration techniques were verified. The vibration pad was placed under the lower back, with the volunteers in the supine position. The results indicated that the PM vibrated well through the transmitted vibration from the lumbar spine, which suggests that the placement of a narrow vibration pad under the supine body, along the lumbar spine, allows the vibration of the PM. The shear modulus of the PM ($n = 7$) was 1.23 ± 0.09 kPa (mean ± SEM) on the right side and 1.22 ± 0.15 kPa on the left side, with no significant difference (t-test, $P > 0.05$). Increased stiffness of the muscle due to continuous local contraction may be an important cause of non-specific low back pain (LBP). The present vibration techniques for MRE of the PM provide a quantitative diagnostic tool for changes in muscle stiffness associated with non-specific LBP.

1. Introduction

Palpation is the manual examination of the body conducted for survey or diagnosis of disease or illness. Palpation is an important part of physical examination, and provides physical information of the organ through the sense of touch. However, palpation is subjective, and deep-lying tissues are not accessible to physicians via palpation. Magnetic resonance elastography (MRE) [1–4] is a relatively new technique that enables the measurement of mechanical properties, such as the shear modulus of different biological tissues in vivo and in the brain [4–8], breast [4,9,10], liver [4,11–13], prostate [14,15], and skeletal muscles [4,16–20]. In MRE, mechanical vibration is applied to the surface of the patient's body, which generates longitudinal and shear waves that travel into the patient's deep tissues. Sound speed of the longitudinal wave is faster (approximately 100–1000 times) than that of the shear wave. Detection of longitudinal wave using MRE is difficult because its wavelength (sound speed = wavelength × frequency) is too long to fit into the human body; therefore, MRE uses only shear waves. Cyclic shear motion synchronized with MR pulse sequence is applied to the tissue of interest using external vibration sources, and the resultant oscillating displacements are captured in MR phase images using bipolar gradient lobes of motion-encoding gradient (MEG) in a conventional MR pulse sequence [1]. This type of MR phase imaging measures the velocity of shear waves and is used to estimate the tissue's shear modulus. MRE considers changes in wavelength caused by changes in the velocity of shear waves. Wave images of shear waves in the MR phase images are converted into images of shear modulus in the elastogram using an inversion algorithm. The local frequency estimate (LFE) algorithm has been routinely used as an inversion algorithm [21]. The amplitudes of the shear waves are damped in proportion to the

Abbreviations: PM, psoas major muscle; LBP, low back pain; ESM, erector spine muscles; MAV, mean oscillation amplitude value

* Corresponding author at: Department of Radiological Science, Graduate School of Human Health Science, Tokyo Metropolitan University, 7-2-10, Higashiogu, Arakawa-ku, Tokyo, Japan.
E-mail address: t-numano@tmu.ac.jp (T. Numano).

https://doi.org/10.1016/j.mri.2019.08.006
Received 4 January 2019; Received in revised form 29 July 2019; Accepted 15 August 2019

depth from the surface. In particular, because of the low amplitudes of the propagating waves in deep tissues, the amount of MR phase shift is decreased, which makes it difficult to detect wavelengths in the wave images. To solve the problem of low amplitudes of shear waves, MEG is used to enhance sensitivity to shear waves in the MR pulse sequence. With regard to MEG, gradient oscillation is synchronous with the vibration frequency, and sensitivity of the MR pulse sequence is proportional to the number and strength of the MEG. Common MRE pulse sequences (MEG-incorporated MRE sequences) have high sensitivity to shear waves, but they also have drawbacks. Because the MEG is applied between radiofrequency (RF) excitation pulse and echo signal acquisition, its inclusion prolongs the echo time (TE). Thus, the TE of common MRE pulse sequences tends to be longer than that of conventional MR pulse sequences and can reduce the signal-to-noise ratio and increases effect of magnetic susceptibility. To overcome difficulties in MRE, we developed a new MEG-less multi-echo MRE sequence [22]. MEG-less multi-echo MRE sequence is the same as the common gradient-echo type multi-echo MR sequence and allows clinicians to perform MRE using conventional MR imaging. The MEG-less multi-echo MRE sequence uses a series of gradient-echoes acquired as a train following a single excitation pulse. The symmetrical bipolar readout gradient (RG) lobes acquire multiple symmetrical gradient-echoes (multi-echo). The RG has a MEG-like effect; if RG is synchronized with the vibration frequency, sequentially generated echoes induce greater MEG-like effects (1st TE image < 2nd TE image < 3rd TE image, and so on).

Low back pain (LBP) has many causes. Non-specific LBP is considered as LBP without a known pathoanatomical cause and is the most common form of LBP [23]. Previous studies have investigated non-specific LBP using conventional MR images (T1- or T2-weighted images) and reported the presence of atrophy of the specific paraspinal muscles and fatty infiltration in patients with acute and chronic LBP, although the mechanisms responsible for this phenomenon were unclear [24–27]. Other studies have investigated the relationships between the size (cross-sectional area [CSA]) of the psoas major muscle (PM) and LBP [26–29] and revealed that patients with LBP had a larger CSA of the PM than controls at the level of the L3/L4 and L4/L5 intervertebral discs [26]. However, another study using X-ray CT images reported that the PM was significantly smaller in patients with LBP at the lower end-plate of L4 [28]. Several studies have focused on non-specific LBP using conventional diagnostic imaging methods, but the results for non-specific LBP have been inconsistent and inconclusive; in contrast, clinical studies have suggested that continuous local muscle contraction that causes increased local stiffness of the muscle is an important cause of non-specific LBP [30,31]. Therefore, a new diagnostic imaging technique is required to identify an imaging biomarker of muscle stiffness that can clarify the etiology of non-specific LBP. MRE has been extensively used to investigate the shear modulus of the skeletal muscles because the muscle stiffness changes according to the contractile state of the muscle; the findings suggest that MRE can be used to assess a new imaging biomarker for LBP. To our knowledge, no previous study has applied MRE of the PM to investigate non-specific LBP. MRE of the PM is an effective method to assess the quantitative stiffness of the deep-lying muscles such as the PM, which may have a role in causing non-specific LBP because manual examination through palpation of the PM is difficult [30].

In the present study, we developed a vibration system for MRE of the PM using MEG-less multi-echo MRE sequence. Because the PM is deep-lying, the transmission of vibrations to the PM is difficult. Therefore, we induced vibration of the lumbar vertebra, which allowed the transmission of shear waves to the PM.

2. Material and methods

2.1. Participants

Seven healthy volunteers (all male; age-range, 20–25 years) were enrolled. The study was approved by our Institutional Ethic Review Board, and all experiments were performed after obtaining written informed consent from each of the participants.

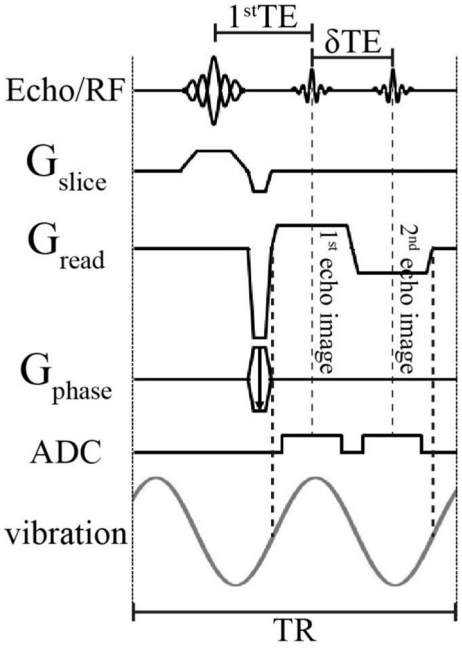

Fig. 1. Sequence diagram for motion encoding gradient (MEG)-less multi-echo magnetic resonance elastography (MRE) sequence. Symmetrical readout gradient lobes generated two gradient echoes, and the interval of the 1st and 2nd echoes was δTE. The magnitude images of the 1st echo time (TE) were used as anatomical structure images, and the MR phase images of the 2nd TE were used as wave images. The vibration pad was continuously oscillating (vibrating) during this sequence, and the vibration frequency was set at an integer multiple of 1/repetition time (TR). The vibration phase offset was controlled by a pneumatic vibration generator.

2.2. MEG-less multi-echo MRE sequence

A diagram of the MEG-less multi-echo MRE sequence is shown in Fig. 1. MEG-less multi-echo MRE sequence acquires images at different weights and/or TEs and allows the acquisition of various images without increasing the acquisition time. Magnitude images of the 1st TE were used as anatomical-structure images, and MR phase images of the 2nd TE were used as wave images. Since the 1st TE signals have the highest SNR and are less affected by magnetic susceptibility artifacts, they provide the best anatomical-structure images because. However, the MR phase image (wave images) of the 1st TE, wave propagation in the PM was not clearly represented due to inadequate MEG-like effects to enable visualization. In the 2nd TE, the wave images represented wave propagation clearly compared with those in the 1st TE because MEG-like effects were sufficient to visualize wave propagation. Because both images were acquired simultaneously, fusion of the two images could be easily obtained without image registration processing. However, the detection of vibration perpendicular to the imaging plane was difficult because the motion-encoding direction depends on the RG direction.

Previously, we presented comparison of quality control homogenous phantom experiments with three MRE sequences (MEG-less multi-echo MRE sequence, gradient-echo type MEG-incorporated MRE sequence, spin echo-EPI type MEG-incorporated MRE sequence) in Japanese Society of Radiological Technology (JSRT2017) [32] and Japanese Society of Magnetic Resonance in Medicine (JSMRM2017) [33]. In the spin echo-EPI type MRE, wavelength changes of the propagating wave according to the direction of image distortion were

present and incorrect value of shear modulus was obtained. The shear modulus of MEG-less multi-echo MRE was almost the same as that of gradient-echo type MRE.

2.3. Experimental setup

All MR imaging (MRI) and MRE experiments were performed using the clinical MR imager, Achieva 3.0 T (Philips Healthcare, Best, The Netherlands) with a SENSE Torso 8-ch coil, with subjects in the supine position. Volunteers were instructed to relax during imaging. A waveform generation system, LabVIEW, USB-6221 (National Instruments, Austin, TX, USA), was used to generate vibration waveforms. To synchronize the vibration with MEG-less multi-echo MRE pulse sequence, the vibration frequency was set at an integer multiple of 1/repetition time (TR), and transistor–transistor logic (TTL) signals from the RF pulse generator of the MRI system were used to trigger the vibration. Sinusoidal waveforms with arbitrary frequencies and phase were generated by the waveform generation system, and the amplitude of sinusoidal waveforms was ± 1 V. The vibration phase offset was controlled by the waveform generator to provide continuous steady-state vibrations throughout the acquisition at each imaging period. A power amplifier, XTi 1000 (Crown, IN, USA), and a pneumatic pressure generator, Subwoofer TIT320C-4 12″ (Dayton Audio, OH, USA), were used to apply vibrations to a vibration pad through a hose. The amplifier was set to the maximum amplification in all experiments. The vibration pad was produced using a three-dimensional (3D) printer (3Dtouch; 3D System, SC, USA) to adapt to the low-back region of the body. Extremely strong vibrations were not used, and the vibration power used was similar to that of electric low-back massagers; thus, the level of patient discomfort was minimum. All MRE image processing was performed using the LFE algorithm freeware, MRE/Wave (MAYO CLINIC, Rochester, MN, USA).

MRE of the PM with vibration frequency of 50 Hz was conducted and synchronized with 10 ms of δTE (gap of the 1st and 2nd TE). Vibration frequency of 50 Hz was selected to offset between penetration depth and resolution of shear modulus in the PM. MR phase images were recorded with the following parameters: acquisition matrix, 512 × 512; scan percentage, 50% (zero-filling interpolation); number of averages, 4; SENSE reduction factor, 2; flip angle, 20°; field of view, 290–350 mm; slice thickness, 10 mm; 1st TE of 2.3 ms, and 2nd TE of 12.3 ms; TR, 40 ms; acquisition time per offset of vibration, 20.5 s (offset of 4 vibration phases; total, 82 s). Axial images were obtained at the L3/L4 level at an angle parallel to the intervertebral disc. The MEG-like effect (readout gradient direction) was set to the anterior-posterior (A-P) direction and the L-R direction.

The PM-MRE setup is shown in Fig. 2. The volunteer was maintained in supine position, and a triangular pillow was placed under the knee to cause bending of the knee joint. Bent knees alleviate physiological curvature of the lumbar spine by preventing roll-back of the lower back. The three-way vibration pad was placed under the lower back of the volunteer in supine position, and secured using a Velcro strap. In addition, a silicon sheet was placed between the vibration pad and the skin of the lower back of the individual. The silicon sheet acts as a substitute for the vibration membrane to prevent air leakage through the gaps between the vibration pad and skin of the lower back. The three-way pad was flexible, and each vibration source (Right, Center, and Left) was connected to a pneumatic pressure generator using a commercial hose. In this study, each vibration source was activated in series.

2.4. Image processing and data analysis

All wave images were processed with phase-unwrapping algorithm and a Gaussian spatial filter, MRE/Wave (MAYO CLINIC, Rochester, MN, USA) after extracting the PM and erector spine muscles (ESM) from the raw data. MRE image processing to generate the oscillation amplitude image and elastogram was performed using MRE/Wave. The regions of interests (ROIs) were set at the PM and ESM on both sides, as shown in Fig. 2a. The ROI was used to measure the mean oscillation amplitude value (MAV) of the propagating shear waves in the PM and ESM (PM-MAV and ESM-MAV) and mean shear modulus of the PM. The MAV was measured from the oscillation amplitude images, and the mean shear modulus was computed from the elastograms. Additionally, the wavelength was measured with calipers in the wave image, and the PM shear modulus (μ) was calculated using Eq. (1) as follows:

$$\mu = \rho f^2 \lambda^2 \quad (1)$$

where ρ is the supraspinatus muscle density (1 g/cm^3), f is the frequency, and λ is the wavelength.

MAV was presented as mean and standard error (SEM). Normality of the data distribution was assessed using the Shapiro–Wilk test. For normal variables, the homogeneity of variance was assessed using the Levene's test. MAV obtained at right-pad activation was analyzed by repeated-measures one-way ANOVA, and Bonferroni's method was used for post-hoc analyses. The Greenhouse–Geisser correction was used for repeated-measures one-way ANOVA because the assumption of sphericity was violated (Mauchly's test of sphericity, $P < 0.05$). MAV at center- and left-pad activation was analyzed using the Friedman test, and the Dunn's method was used for post-hoc analyses. All data analyses were performed using Statistical Package for the Social Sciences (SPSS) version 19.0 (IBM Inc., New York, USA). $P < 0.05$ was considered as statistically significant.

Shear modulus data was presented as mean ± SEM. Normality of the data distribution was assessed using the Shapiro–Wilk test. The homogeneity of variance in all normal variables was assessed using the Levene's test. All shear modulus data were analyzed using two-way ANOVA. All data analyses were performed using SPSS. $P < 0.05$ was considered as statistically significant.

3. Results

3.1. MEG-like effect direction

The results of preliminary experiment to determine suitable direction of the MEG-like effect for the PM are shown in Fig. 3; changes in the wave propagation pattern according to the direction of the MEG-like effect are observed. The vibration pad was placed at the center of the back in each volunteer maintained in supine position, and ROIs were placed in the PM at both sides to measure MAVs of propagating shear waves in the PM (Fig. 3a). The vibration direction of the lumbar spine is shown in Fig. 3b. The lumbar spine are fixed in the vertical direction by the anterior longitudinal ligament, posterior longitudinal ligament, and facet joints; hence, the vibration penetrated from the posterior (P) to the anterior (A) sides, and vibration of the lumbar spine was observed predominantly in the A-P direction. Wave images at the two different directions of the MEG-like effect in the PM and ESM are shown in Fig. 3c and d; these wave images were overlaid on the magnitude images of MR (Fig. 3a). Comparisons between the mean PM-MAV ($n = 7$) at each direction of the MEG-like effect are shown in Fig. 4. Normality of the data distribution was assessed using the Shapiro–Wilk test. The MAV data of the PM at right side were analyzed using two-sample t-test and significant difference was obtained ($P < 0.01$). The MAV data of the PM at left side were analyzed using the Wilcoxon signed ranks test, and significant difference was obtained ($P = 0.018$). The MAV at the A-P direction was higher than that at the left-right (L-R) direction in both PMs.

3.2. Three-way vibration pad

Representative wave images obtained by activating each vibration pad of the three-way pad in one volunteer are shown in Fig. 5. The three-way pad was placed at the center of the back of the volunteer in

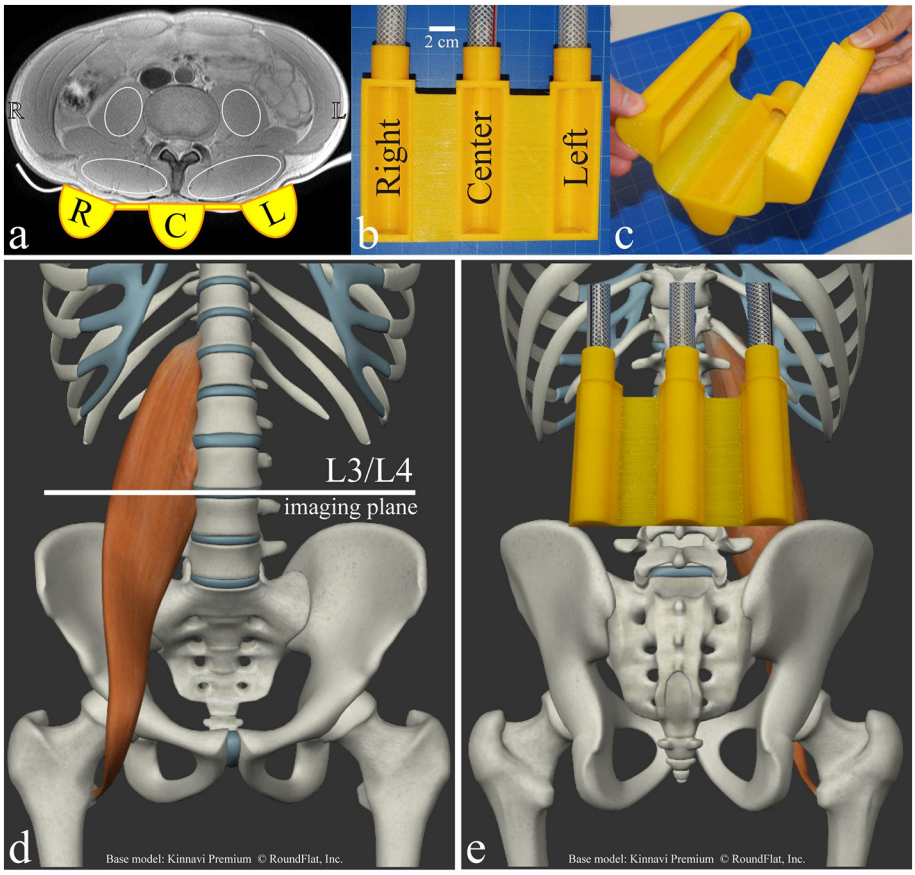

Fig. 2. Anatomical relationships among the vibration pad, psoas major muscle (PM), and lumbar skeleton. (a) Representative axial image of the low-back region (L3/L4) in a volunteer in supine position with three-way vibration pad placed under the back. R, right; C, center; L, left. White circles are the regions of interests (ROIs) in this study. ROIs were set at the PM and elector spine muscles (ESMs) at both sides. (b) Three-way pad made with 3D printer. Connection of each vibration pad (R, C, L) to the pneumatic pressure generator using a commercial hose, and sequential activation of each pad. (c) Flexibility of the three-way pad. (d) Anatomical structure of the PM and imaging plane. (e) Placement of the three-way pad below the lumbar spine.

supine position. Chromas of the wave images were considered to indicate the amplitudes and the crest and trough of propagating shear waves in the PM and ESM. In case of right-pad activation (Fig. 5d), brighter chromas at the right versus left side of the PM were observed. In case of center-pad activation (Fig. 5e), bilaterally symmetrical patterns of chromas of the wave images at the PM were observed. In case of left-pad activation (Fig. 5f), brighter chromas at the left versus right side of the PM were obtained. Similar results were obtained in all volunteers ($n = 7$).

Comparisons of the mean PM- and ESM-MAVs ($n = 7$) under activation of each pad are shown in Fig. 6. In case of right-pad activation (Fig. 6a), significant main effect (repeated measures one-way ANOVA; F

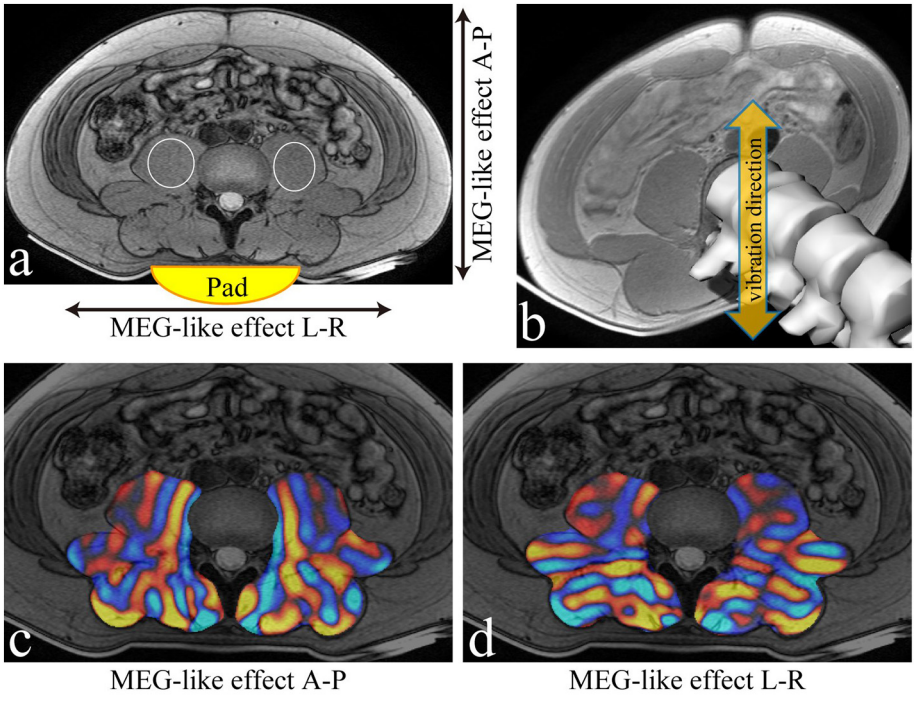

Fig. 3. Results of the preliminary experiment to determine the suitable direction of the motion encoding gradient (MEG)-like effect. (a) Position of the vibration pad and directions of MEG-like effects. White circles are the regions of interests (ROIs) in this study. ROIs at the psoas major muscle (PM) on both sides. (b) The direction of oscillation of the lumbar spine induced by movements of the vibration pad. (c, d) Wave images made by the fusion of masked (elector spine muscles (ESM) and PM) wave images with magnitude images of the 1st echo time (TE) based on the A-P (c) and left-right (L-R) directions of the MEG-like effect. (d).

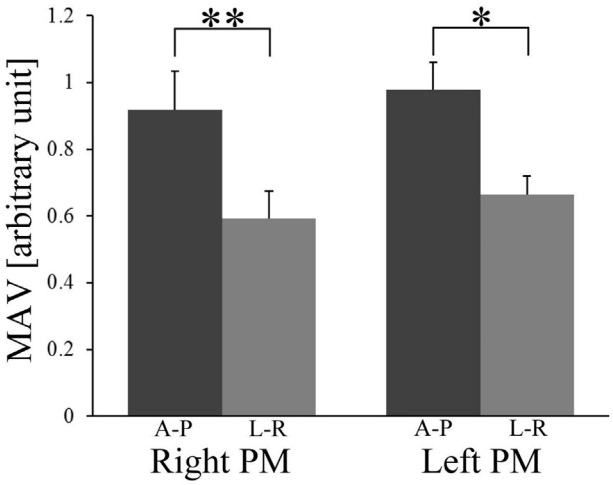

Fig. 4. Mean oscillation amplitude value (MAV) of the psoas major muscle (PM) at both directions of the MEG-like effect. Error bars indicate standard errors. **, *, significant difference at $P < 0.01$, $P < 0.05$, respectively.

[1.08, 6.45] = 27.82, $P < 0.01$) was obtained, and in the post-hoc comparisons, higher values of ESM-MAV at the right versus left side ($P < 0.05$), and higher values of those versus PM-MAVs at the right and left sides were obtained ($P < 0.01$). In case of left-pad activation (Fig. 6c), significant difference in the MAV among the three muscles groups was obtained (Friedman test, $P < 0.01$), and in post-hoc comparisons, higher values of both PM- and ESM-MAVs on the left versus right side were obtained ($P < 0.05$); ESM-MAVs at the left side was larger than the PM-MAVs at the right side ($P < 0.01$). In case of center-pad activation (Fig. 6b), significant difference in MAV among the four muscles groups was obtained (Friedman test, $P < 0.01$), and in post-hoc comparisons, no significant difference in the PM- and ESM-MAV between the right and left sides was obtained ($P > 0.05$); the ESM-MAV at both sides was larger than the PM-MAV at both sides ($P < 0.05$). In further data analysis of the PM in Fig. 6, repeated-measures two-way ANOVA including factors of the side of the muscle and position of the activated pad was conducted, since normal distribution of the PM-MAVs was observed; as a result, position was a significant main effect (F[1.15, 6.90] = 21.08, $P < 0.01$). In post-hoc comparisons, larger PM-MAVs were observed at center-pad activation than those at right- ($P < 0.01$) and left- ($P < 0.05$) pad activation. In addition, significant interaction between side and position (F[2, 12] = 7.66, $P < 0.01$) was calculated. In post-hoc comparisons, larger PM-MAVs were observed in the L-PM than in the R-PM ($P < 0.01$) at left-pad activation and in the R-PM than in the L-PM ($P < 0.05$) at right-pad activation. However, no significant difference was obtained in the PM-MAVs between the R-PM and L-PM at center-pad activation.

The average shear modulus from the LFE of elastograms and calipers is summarized as a plot in Fig. 7. In both methods, no significant difference in the shear modulus at each vibration pad was observed ($P > 0.05$). Values of the shear modulus through the LFE of elastograms and calipers in each subject are shown in Table 1. Individual elastograms for the PM at center-pad activation in seven volunteers is shown in Fig. 8. In all subjects, the elastogram was overlaid on the corresponding magnitude image.

4. Discussion

We developed an MRE technique with applicability in the PM using conventional MRI sequence. The proposed MRE technique showed capability to successfully image wave propagation in the PM at the A-P readout direction of the MEG-like effect and axial (transverse) imaging plane under the activation of the center vibration pad. We discussed the conditions (direction of the MEG-like effect and three-way vibration pad) and limitations of the study.

4.1. Direction of the MEG-like effect

Studies have reported that shear wave displacements were induced primarily perpendicular to the muscle fibers because of anisotropy of the muscles [21,34]. Moreover, other studies have demonstrated that the shear wave velocity depends on the direction of wave propagation against that of the muscle fibers [35,36]. Because MRE allows for the visualization of tissue displacements due to vibrations in the MEG direction, the selection of MEG direction is very important in the skeletal muscle MRE. The amplitude of the propagating wave is easily attenuated in vivo, and hence, large MAV should be obtained in all MRE. In this study, MAV was increased at the A-P direction of the MEG-like effect. The vibration pad placed in the low-back region generated compressional wave (Fig. 3a) and it induced micro-displacement of lumbar spine. Because the lumbar spine held in position by the ligaments and joints have movement in the rigid-body mode in vivo, the micro-displacement direction of the lumbar spine was dominantly A-P (Fig. 3b). The PM is a long fusiform muscle located adjacent to the lumbar region of the vertebral column and brim of the lesser pelvis. The findings of our study suggest that the lumbar spine micro-displacement in the A-P direction induced shear waves in the bilateral PM. Because the PM tissue was displaced in the A-P direction and the MAV at A-P

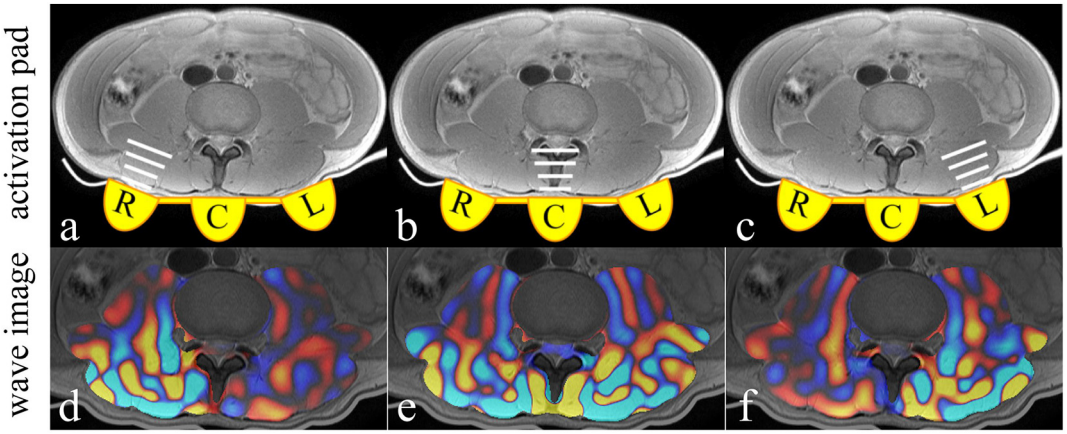

Fig. 5. Wave images obtained by activation of each vibration pad of the three-way pad in one volunteer. (a, b, c) Schema of activation of the right (a) center (b) and left (c) pads. (d) Wave image during activation of the right vibration pad. (e) Wave image during activation of the center vibration pad. (f) Wave image during activation of the left vibration pad.

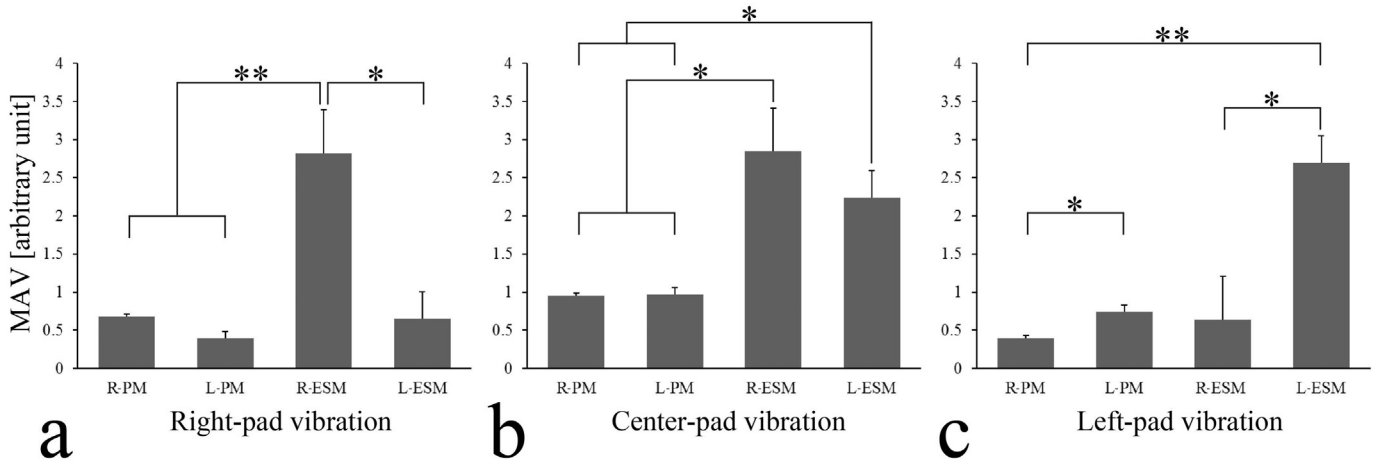

Fig. 6. Mean oscillation amplitude value (MAV) of the psoas major muscle (PM) and elector spine muscles (ESM). (a) Comparison of MAVs at right-pad activation. (b) Comparison of MAVs at center-pad activation. (c) Comparison of MAVs at left-pad activation. Error bars indicate standard errors. **, *, significant difference at $P < 0.01$, $P < 0.05$, respectively.

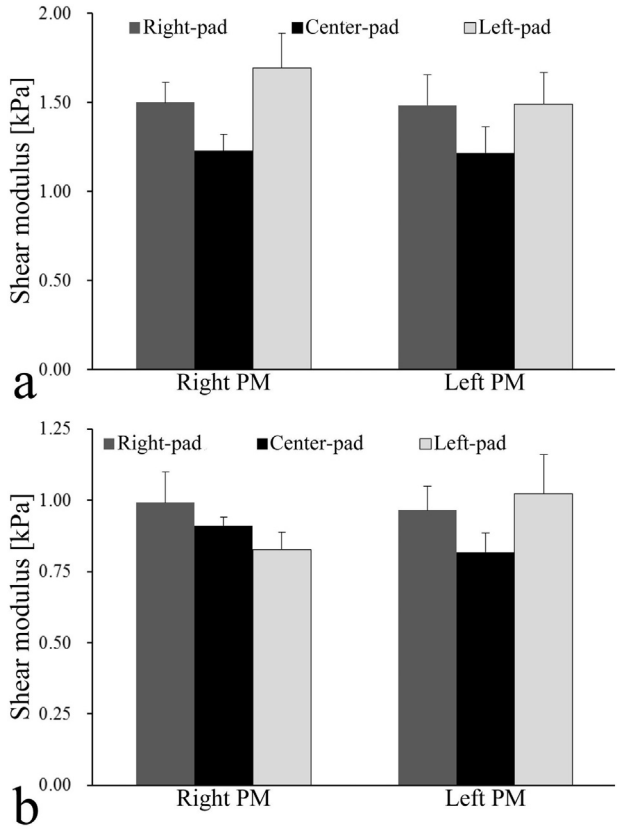

Fig. 7. Shear modulus of the psoas major muscle (PM). (a) Comparison of shear modulus through LFE of elastogram among different vibration-pad positions. Gray bar graph shows result at right-pad activation. Black bar graph shows result at center-pad activation. White bar graph shows result at left-pad activation. There was no significant difference at each pad. (b) Comparison of shear modulus through calipers. Calipers represent manual wavelength measurement on the wave image; values obtained are used to calculate the shear modulus. Gray bar graph shows result at right-pad activation. Black bar graph shows result at center-pad activation. White bar graph shows result at left-pad activation. There was no significant difference at each pad.

was higher than that at L-R (Fig. 4), we considered that the A-P direction of the MEG-like effect was well suited for PM-MRE. Moreover, the MEG-like effect at the A-P direction forms a ripple-like wave pattern from the lumbar spine (Fig. 3c), suggesting that the vibration of the PM was mainly transmitted from the lumbar spine.

4.2. Three-way vibration pad

First, the ESM-MAVs were larger on the activated side than the contralateral non-activated side (Fig. 6a, b), which suggested that vibrations of the ESM were directly transmitted from the activated vibration pad. In contrast, the PM-MAVs were smaller than the ESM-MAVs on the activated sides, and larger at center-pad activation than at right- and left-pad activation. These findings suggested that indirect vibration through the lumbar spine may be a major source of vibration in the PM, especially at center-pad activation; the pad vibration was effectively transmitted to the lumbar spine and subsequently to the PM. However, in case of right- or left-pad activation, PM-MAVs were larger on the activated side than on the contralateral non-activated side, suggesting that indirect vibration through the lumbar spine may have been influenced by direct vibration of the ESM induced by the ipsilateral vibration pad.

Second, ESM-MAV showed large variance, and data distribution was not normal even at center-pad activation (R-ESM and L-ESM; center-pad in Fig. 6b). The large variance of data may be due to mispositioning of the three-way pad. We experienced difficulty in placing the three-way pad at the mid-line of volunteers. For the placement of the three-way pad at the mid-line, we used the spinous process of the lumbar spine as an indicator that can be palpated from the body surface. However, the direction of the spinous process of the lumbar spine differed among volunteers: in volunteer A (Fig. 8a), the spinous process of the lumbar spine protruded slightly to the right, which may have caused the ESM to directly vibrate at center-pad activation from the misplaced vibration pad offset in the horizontal direction. Variation of the spinous process may be an important influencing factor of the large variance of ESM-MAV. In contrast, there was no significant difference in the PM-MAVs between the right and left sides at center-pad activation (R-PM vs. L-PM; Fig. 6b), despite possible misplacement of the center vibration pad. These findings suggest that center-pad activation can generate stable vibration in the PM.

4.3. Shear modulus and the muscle fiber directions

The shear modulus calculated using LFE was approximately 1.5-fold higher than that calculated using calipers. With calipers, the value was obtained through wavelength in the arbitrary profile direction. With LFE, the value was estimated through filters that are a product of radial and directional components [21]. Briefly, the LFE processes of MRE/

Table 1
Mean shear modulus (in kPa) of the PM for all subjects at each vibration-pad activation. Local frequency estimate (LFE) is the value of the shear modulus in the elastogram. Calipers are used to calculate the shear modulus from manual wavelength measurement on the wave image.

	Right PM [kPa]						Left PM [kPa]					
	Right-pad		Center-pad		Left-pad		Right-pad		Center-pad		Left-pad	
	LFE	Calipers	LFE	Calipers	LFE	Calipers	LFE	Calipers	LFE	Calipers	LFE	Calipers
Volunteer 1	1.80	0.64	1.12	0.87	1.44	0.80	1.40	0.68	0.90	0.70	1.31	0.85
Volunteer 2	1.79	0.85	1.15	0.90	2.11	1.07	2.40	Unmeasurable	1.21	0.61	1.99	0.75
Volunteer 3	1.30	1.22	1.25	0.93	1.05	0.90	1.03	0.72	1.75	0.82	1.00	1.04
Volunteer 4	1.01	0.80	0.98	0.82	0.99	0.82	1.89	Unmeasurable	0.82	0.70	1.04	0.62
Volunteer 5	1.36	0.93	1.72	0.90	1.59	1.25	1.64	0.67	1.71	1.04	1.55	1.07
Volunteer 6	1.49	1.04	1.10	1.08	1.17	0.93	1.22	0.98	1.26	1.07	2.23	1.73
Volunteer 7	1.74	1.48	1.28	0.88	2.04	0.99	2.26	1.08	0.87	0.80	1.33	1.11
Average	1.50	0.99	1.23	0.91	1.48	0.97	1.69	0.83	1.22	0.82	1.49	1.02
SEM	0.11	0.11	0.09	0.03	0.17	0.06	0.20	0.09	0.15	0.07	0.18	0.14

All "Caliper" columns are calculated shear modulus [kPa] from each measured wavelength with Eq. (1).
Unmeasurable: inability to measure the wavelength in the wave image.

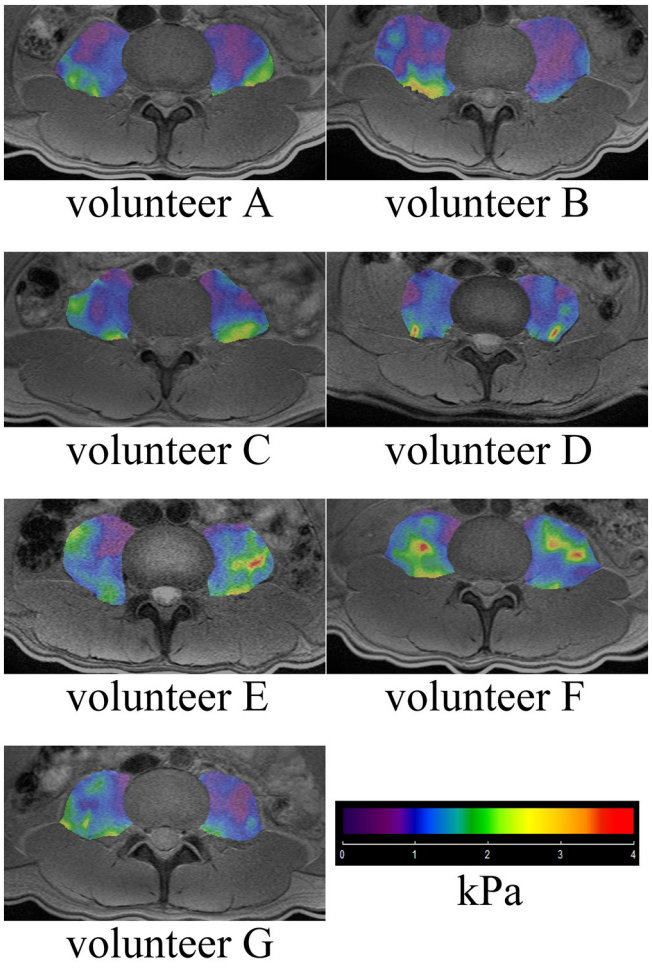

Fig. 8. Elastograms of the psoas major muscle (PM) made by fusion of the masked elastograms with the magnitude images at 1st echo time (TE) in individual volunteers. All elastograms were derived from center-pad activation. The mean shear modulus of the PM ($n = 7$) was 1.23 ± 0.09 kPa (mean ± SEM) on the right side and 1.22 ± 0.15 kPa on the left side.

Wave were along to several directions, and perform weighted averaging on those (directions) results. The difference in the shear modulus was influenced by this weighted averaging. At right-pad activation, we experienced difficulty in reading the wavelength in the left PM with calipers (Table 1) due to interference of the vibration from the LV during right-pad vibration. In contrast, in case of vibration at center-pad activation, we were able to easily read the wavelength due to less interference from vibration at side-pad activation. Thus, center-pad activation is suitable for PM-MRE and prevents interference due to vibration from the side-pad.

In cases of homogeneous isotropic elastic tissues such as the liver tissue, there is little difference in the shear modulus according to the MEG direction, whereas, in cases of anisotropic elastic tissues such as the muscle tissues, the propagating wave speed (wavelength) is dependent on the muscle fiber direction. Therefore, the measurement value of the shear modulus may change according to the measurement direction of the wavelength. In this study, we measured the wavelength perpendicular to the muscle fibers, which appears shorter than that obtained in the parallel direction. A previous study [36] has reported a difference in the shear modulus in the medial gastrocnemius (parallel: 0.86 ± 0.15 kPa, perpendicular: 0.66 ± 0.19 kPa), soleus (parallel: 0.83 ± 0.22 kPa, perpendicular: 0.65 ± 0.13 kPa), and tibialis anterior (parallel: 0.78 ± 0.24 kPa, perpendicular: 0.66 ± 0.16 kPa). Based on the previously reported values of different muscles, we considered that data of the shear modulus of the PM in our study had no outliers.

4.4. Study limitations

First, the sample size of the study was small ($n = 7$). Further studies including a larger sample size are needed to evaluate shear modulus in populations of different ages. Second, wave images derived from the MEG-like effect perpendicular to the axial plane could not be obtained, and because axial image at only the A-P direction of the MEG-like effect was acquired, measurement of the actual shear modulus may have been prevented. However, because the vibration pads stimulated the lumbar spine in the A-P direction, and the PM is located adjacent to the lumbar spine, displacement of the PM in the A-P direction is expected. From the view point of anatomy, it is difficult to vibrate the lumber spine at the head-feet (H—F) direction, and assessment of the PM should be performed in the A-P direction of the MEG-like effect although the H—F direction is not optimal. Third, vibration frequency of only 50 Hz was used in this study. A higher vibration frequency would improve the resolution of the elastogram because of the shorter wavelength, and the resolution was higher at 75 Hz than at 50 Hz [4,21]. A lower vibration frequency would improve the penetration depth of shear waves because of the longer wavelength; the penetration depth was higher at 50 Hz than at 75 Hz [4,21]. The best vibration frequency for a particular application depends on offsetting these values. At the vibration frequency of 75 Hz, the shear waves did not reach the distal PM in some volunteers (data not shown). In order to implement a robust PM-MRE that is

less dependent on the body type or size of the examinees, a vibration frequency of 50 Hz is considered as suitable.

5. Conclusions

We demonstrated the successful application of PM-MRE. Our results revealed that wave images showed wave propagation under the following conditions: A narrow vibration pad placed under the body of the individual in the supine position, along the lumbar spine; axial image at the level of L3/L4; and MEG-like effect in the A-P direction. Further studies with a large sample size are required to determine the mean MAV in the PM in populations of different ages, which would enable the objective diagnosis of non-specific LBP.

Funding

This work was supported by JSPS KAKENHI Grant Number JP19K09579, Japan.

References

[1] Muthupillai R, Lomas DJ, Rossman PJ, Greenleaf JF, Manduca A, Ehman RL. Magnetic resonance elastography by direct visualization of propagating acoustic strain waves. Science 1995;269:1854–7.
[2] Muthupillai R, Ehman RL. Magnetic resonance elastography. Nat Med 1996;2:601–3.
[3] Muthupillai R, Rossman PJ, Lomas DJ, Greenleaf JF, Riederer SJ, Ehman RL. Magnetic resonance imaging of transverse acoustic strain waves. Magn Reson Med 1996;36:266–74.
[4] Mariappan YK, Glaser KJ, Ehman RL. Magnetic resonance elastography: a review. Clin Anat 2010;23:497–511.
[5] Liu GR, Gao PY, Lin Y, Xue J, Wang XC, Sui BB, et al. Brain magnetic resonance elastography on healthy volunteers: a safety study. Acta Radiol 2009;50:423–9.
[6] Di Ieva A, Grizzi F, Rognone E, Tse ZT, Parittotokkaporn T, Rodriguez YBF, et al. Magnetic resonance elastography: a general overview of its current and future applications in brain imaging. Neurosurg Rev 2010;33:137–45. [discussion 45].
[7] Latta P, Gruwel ML, Debergue P, Matwiy B, Sboto-Frankenstein UN, Tomanek B. Convertible pneumatic actuator for magnetic resonance elastography of the brain. Magn Reson Imaging 2011;29:147–52.
[8] Johnson CL, McGarry MD, Van Houten EE, Weaver JB, Paulsen KD, Sutton BP, et al. Magnetic resonance elastography of the brain using multishot spiral readouts with self-navigated motion correction. Magn Reson Med 2013;70:404–12.
[9] Plewes DB, Bishop J, Samani A, Sciarretta J. Visualization and quantification of breast cancer biomechanical properties with magnetic resonance elastography. Phys Med Biol 2000;45:1591–610.
[10] Sinkus R, Lorenzen J, Schrader D, Lorenzen M, Dargatz M, Holz D. High-resolution tensor MR elastography for breast tumour detection. Phys Med Biol 2000;45:1649–64.
[11] Rouviere O, Yin M, Dresner MA, Rossman PJ, Burgart LJ, Fidler JL, et al. MR elastography of the liver: preliminary results. Radiology 2006;240:440–8.
[12] Venkatesh SK, Yin M, Glockner JF, Takahashi N, Araoz PA, Talwalkar JA, et al. MR elastography of liver tumors: preliminary results. AJR Am J Roentgenol 2008;190:1534–40.
[13] Talwalkar JA, Yin M, Fidler JL, Sanderson SO, Kamath PS, Ehman RL. Magnetic resonance imaging of hepatic fibrosis: emerging clinical applications. Hepatology 2008;47:332–42.
[14] Arani A, Plewes D, Krieger A, Chopra R. The feasibility of endorectal MR elastography for prostate cancer localization. Magn Reson Med 2011;66:1649–57.
[15] Sahebjavaher RS, Baghani A, Honarvar M, Sinkus R, Salcudean SE. Transperineal prostate MR elastography: initial in vivo results. Magn Reson Med 2013;69:411–20.
[16] Dresner MA, Rose GH, Rossman PJ, Muthupillai R, Manduca A, Ehman RL. Magnetic resonance elastography of skeletal muscle. J Magn Reson Imaging 2001;13:269–76.
[17] Bensamoun SF, Ringleb SI, Littrell L, Chen Q, Brennan M, Ehman RL, et al. Determination of thigh muscle stiffness using magnetic resonance elastography. J Magn Reson Imaging 2006;23:242–7.
[18] Ito D, Numano T, Mizuhara K, Takamoto K, Onishi T, Nishijo H. A new technique for MR elastography of the supraspinatus muscle: a gradient-echo type multi-echo sequence. Magn Reson Imaging 2016;34:1181–8.
[19] Creze M, Soubeyrand M, Yue JL, Gagey O, Maitre X, Bellin MF. Magnetic resonance elastography of the lumbar back muscles: a preliminary study. Clin Anat 2018;31:514–20.
[20] Ito D, Numano T, Takamoto K, Ueki T, Habe T, Igarashi K, et al. Simultaneous acquisition of magnetic resonance elastography of the supraspinatus and the trapezius muscles. Magn Reson Imaging 2018;57:95–102.
[21] Manduca A, Oliphant TE, Dresner MA, Mahowald JL, Kruse SA, Amromin E, et al. Magnetic resonance elastography: non-invasive mapping of tissue elasticity. Med Image Anal 2001;5(4):237–54.
[22] Numano T, Mizuhara K, Hata J, Washio T, Homma K. A simple method for MR elastography: a gradient-echo type multi-echo sequence. Magn Reson Imaging 2015;33:31–7.
[23] Maher C, Underwood M, Buchbinder R. Non-specific low back pain. Lancet 2017;389:736–47.
[24] Mengiardi B, Schmid MR, Boos N, Pfirrmann CW, Brunner F, Elfering A, et al. Fat content of lumbar paraspinal muscles in patients with chronic low back pain and in asymptomatic volunteers: quantification with MR spectroscopy. Radiology 2006;240:786–92.
[25] D'Hooge R, Cagnie B, Crombez G, Vanderstraeten G, Dolphens M, Danneels L. Increased intramuscular fatty infiltration without differences in lumbar muscle cross-sectional area during remission of unilateral recurrent low back pain. Man Ther 2012;17:584–8.
[26] Arbanas J, Pavlovic I, Marijancic V, Vlahovic H, Starcevic-Klasan G, Peharec S, et al. MRI features of the psoas major muscle in patients with low back pain. Eur Spine J 2013;22:1965–71.
[27] Wan Q, Lin C, Li X, Zeng W, Ma C. MRI assessment of paraspinal muscles in patients with acute and chronic unilateral low back pain. Br J Radiol 2015;88:20140546.
[28] Danneels LA, Vanderstraeten GG, Cambier DC, Witvrouw EE, De Cuyper HJ. CT imaging of trunk muscles in chronic low back pain patients and healthy control subjects. Eur Spine J 2000;9:266–72.
[29] Kamaz M, Kiresi D, Oğuz H, Emlik D, Levendoğlu F. CT measurement of trunk muscle areas in patients with chronic low back pain. Diagn Interv Radiol 2007;13:144–8.
[30] Ingber RS. Iliopsoas myofascial dysfunction: a treatable cause of "failed" low back syndrome. Arch Phys Med Rehabil 1989;70:382–6.
[31] Iglesias-González JJ, Muñoz-García MT, Rodrigues-de-Souza DP, Alburquerque-Sendín F, Fernández-de-Las-Peñas C. Myofascial trigger points, pain, disability, and sleep quality in patients with chronic nonspecific low back pain. Pain Med 2013;14:1964–70.
[32] Numano T, Seino S, Kanazawa T, Kanezawa T, Nojima Y, Igarashi K, et al. Operation of a dedicated vibration pad of the standard MR elastography phantom. Proceedings of the 73rd Annual Meeting of the Japanese Society of Radiological Technology (JSRT). 2017 April 13-16. [Yokohama, Japan].
[33] Numano T, Seino S, Kanazawa T, Kanezawa T, Nojima Y, Igarashi K, et al. Development and operation of the dedicated vibration pad of the quality control MR elastography phantom. Proceedings of the 45th Annual Meeting of the Japanese Society of Magnetic Resonance in Medicine (JSMRM); 2017 Sep 14–16; Utsunomiya, Japan.
[34] Debernard L, Robert L, Charleux F, Bensamoun SF. Characterization of muscle architecture in children and adults using magnetic resonance elastography and ultrasound techniques. J Biomech 2011;44:397–401.
[35] Gennisson JL, Catheline S, Chaffai S, Fink M. Transient elastography in anisotropic medium: application to the measurement of slow and fast shear wave speeds in muscles. J Acoust Soc Am 2003;114:536–41.
[36] Green MA, Geng G, Qin E, Sinkus R, Gandevia SC, Bilston LE. Measuring anisotropic muscle stiffness properties using elastography. NMR Biomed 2013;26:1387–94.